Kovove Mater. 62 2024 147–152
DOI: 10.31577/km.2024.3.147

Effect of electric field on high-temperature decarburization of 0.9%C-Fe steel

Feng-Fang Liu[1,2], Ming-Long Gong[1,2]*, Jing Bai[1,2], Qiu-Zhi Gao[1,2]

[1]*School of Materials Science and Engineering, Northeastern University, Shenyang 110819, P. R. China*
[2]*Key Laboratory of Advanced Metal Materials and Forming Technology in Qinhuangdao, Northeastern University at Qinhuangdao Branch, Qinhuangdao 066004, P. R. China*

Received 25 March 2024, received in revised form 10 May 2024, accepted 25 May 2024

Abstract

0.9%C-Fe steel specimens were heated to 930 °C in air ovens with and without applying electric fields. The study reveals that electric field annealing leads to an augmented thickness of the fully decarburized layer on the surface of the specimen, as well as an increased volume fraction of proeutectoid ferrite in the specimen's center. This phenomenon arises from the accelerated diffusion rate of carbon atoms to the specimen's surface induced by the electric field, thereby enhancing the decarburization process.

K e y w o r d s: electric field, 0.9%C-Fe steel, decarburization

1. Introduction

The influence of an applied potential field on atomic diffusion is significant. For instance, free energy disparities on the sample surface drive atomic diffusion when subjected to stress and temperature fields. Among external physical fields, the electric field particularly affects atom diffusion [1–6]. When a sample is connected to the positive terminal of an external power source, a positive charge layer forms on its surface. Under the external electric field's influence, negatively charged vacancies migrate toward the metal surface, expediting the atom diffusion process.

Liu et al. [7–9] performed electric field homogenization annealing on 2091Al-Li-Cu-Mg alloy. The findings demonstrate that this treatment accelerates the diffusion of Cu and Mg atoms, thereby promoting the dissolution of the second phase and reducing its volume percentage. Additionally, prolonged application of the external electric field during homogenization causes Mg atoms in the surface layer to diffuse upward, resulting in a slight increase in the percentage of the second phase volume in the surface layer while decreasing in the center. Lu et al. [10] investigated the impact of the electric field on the aging process of low-carbon steel, revealing its inhibition of the precipitation process and significant alteration of the size, morphology, and distribution of precipitates near and within grain boundaries. Fu et al. [11] explored the diffusion behavior of friction-welded joints of copper and stainless steel during electric field heat treatment, noting a higher diffusion coefficient of Fe element at the friction welding interface at 600 °C compared to traditional post-weld heat treatment while also observing a reduction in the diffusion coefficient and diffusion activation energy of Fe element at the welding interface with increasing electric field intensity, particularly evident under negative electric fields. Lu et al. [12] investigated the effect of an external electric field on atomic diffusion behavior at the W/NiFe interface, revealing a decrease in the d orbital electron concentration of W and Ni atoms, consequently lowering the vacancy formation energy and solute atom migration energy. As a result, the diffusion activation energy, composed of vacancy generation energy and solute atom migration energy, decreases, increasing the interface atomic diffusion coefficient. Although the application of electric fields in metal processing and heat treatment has been extensively studied, there is limited research on the decarburization of high-carbon steel under DC electric fields. This study examines the impact of electric fields on the high-temperature decarburization of 0.9%C-Fe

*Corresponding author: tel./fax: +86 15230357760; e-mail address: gongminglong@qhd.neu.edu.cn

Table 1. Chemical composition (wt.%) of material employed in this study – 0.9%C-Fe

C	Si	Mn	P	S	Cu	Fe
0.89	0.23	0.19	0.004	0.013	0.036	Bal.

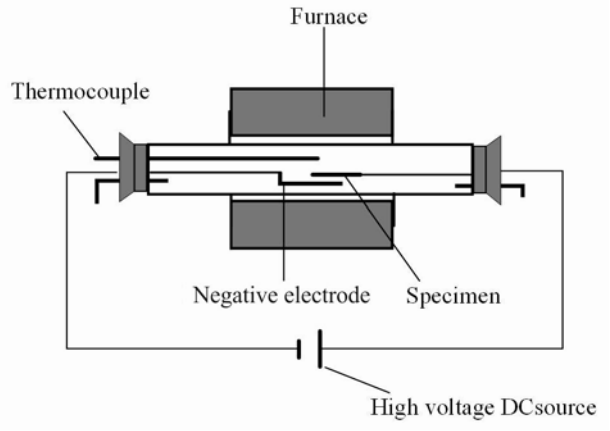

Fig. 1. Schematic of electric field heat treatment furnace.

steel and evaluates the decarburization mechanism under electric field influence.

2. Experimental procedure

The chemical composition of 0.9%C-Fe utilized in this study is delineated in Table 1. The steel under investigation was produced in a vacuum induction furnace. Following casting a 10 kg ingot, it was subsequently forged into a rectangular form measuring $30 \times 100 \times 350\,\mathrm{mm}^3$. Thin slice samples measuring $2 \times 10 \times 20\,\mathrm{mm}^3$ were derived from the forged cuboid material through wire-cutting techniques. Before electric field annealing, the upper and lower surfaces of the samples were polished to an 800# finish using water sandpaper to eliminate any burrs and edges, thereby mitigating the risk of discharge during the electric field annealing process.

During the electric field annealing experiment, the sample was connected in parallel with a stainless steel electrode plate and linked to the positive and negative terminals of the high-voltage DC power supply (as illustrated in Fig. 1). Simultaneously, a custom-made ceramic holder was employed to ensure insulation between the sample and the negative plate.

The heat treatment procedure is outlined in Fig. 2. The sample was heated to 930 ℃, held at this temperature for 6 h, subsequently cooled to 400 ℃ within the furnace, and then air cooled to ambient temperature.

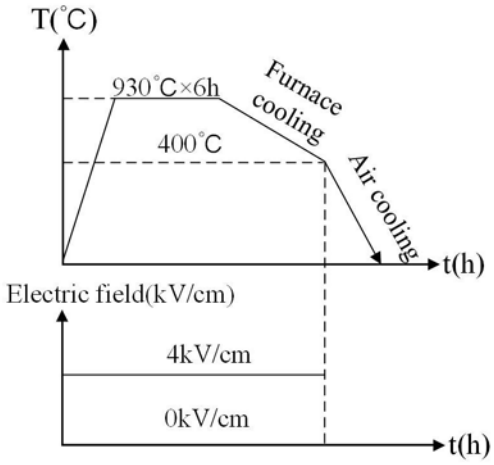

Fig. 2. Heat treatment techniques with and without electric field.

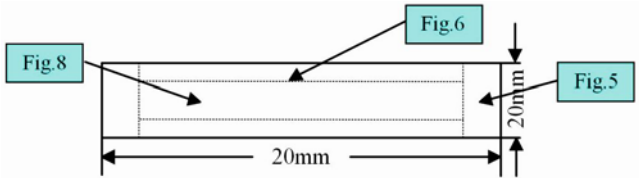

Fig. 3. Schematic illustration of the positions observed for the specimens.

No protective gas was employed during the heat treatment process. For the application of an electric field, the electric field intensity was set to $4\,\mathrm{kV\,cm}^{-1}$. Figures 1 and 2 depict the electric and non-electric field heat treatment experiments, respectively. In the case of electric heat treatment furnaces, apart from the absence of electric field intensity, the process parameters for electric field annealing remained consistent with those applied in non-electric field annealing, ensuring the comparability of test outcomes. The microstructure of the treated samples was examined utilizing a LEICA DMI5000m inverted metallographic microscope, with the observation surface being the lateral aspect of the sample, as delineated in Fig. 3.

3. Results

Figure 4 depicts the microstructure of 0.9%C-Fe steel after forging. Microscopic examination reveals the presence of coarse pearlite and secondary cementite along the original austenite grain boundaries within 0.9%C-Fe.

Figure 5 illustrates the microstructure observed at both ends of the 0.9%C-Fe steel sample (indicated by the arrow in Fig. 3) following a 6-hour exposure

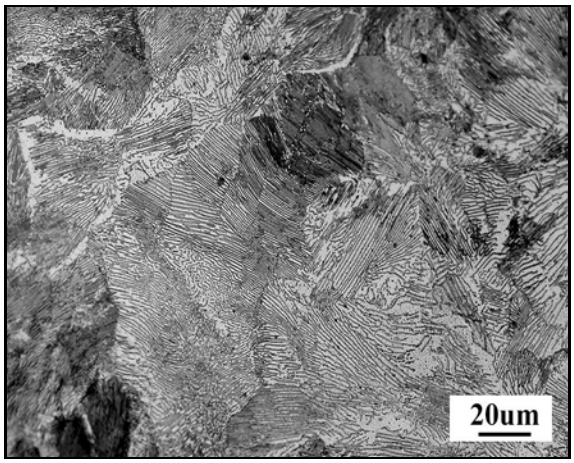

Fig. 4. As-forged microstructure of 0.9%C-Fe steel.

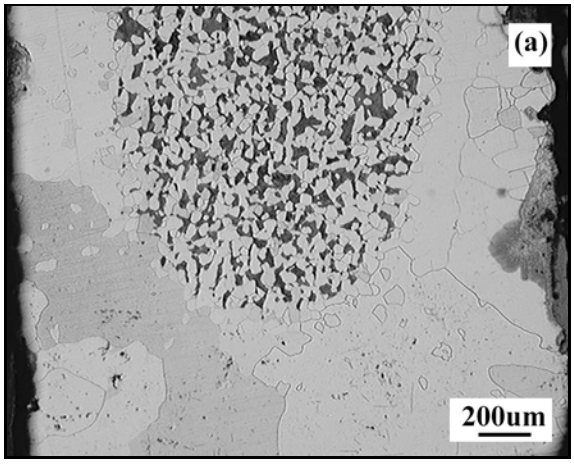

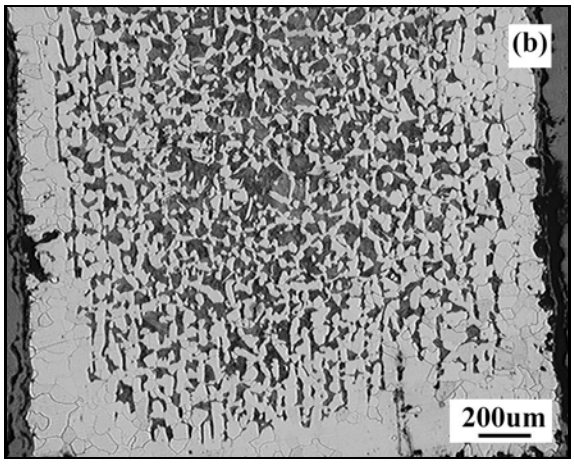

Fig. 5. Microstructures of 0.9%C-Fe steel ends heated at 930 °C for 6 h: (a) $E = 4\,\mathrm{kV\,cm^{-1}}$ and (b) $E = 0\,\mathrm{kV\,cm^{-1}}$.

at 930 °C. It is evident that the average thickness of the fully decarburized layer, influenced by the electric field, measures 553 μm (based on a single field of view,

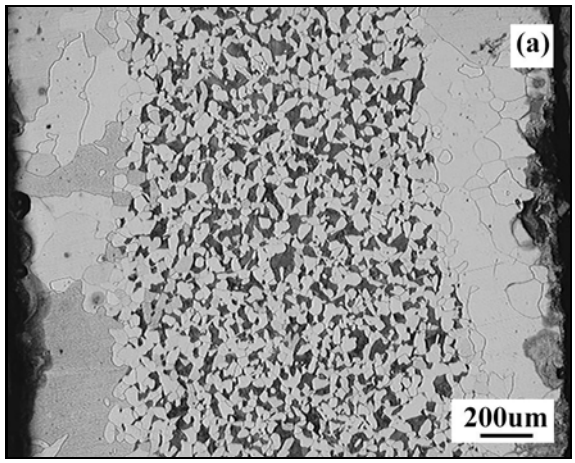

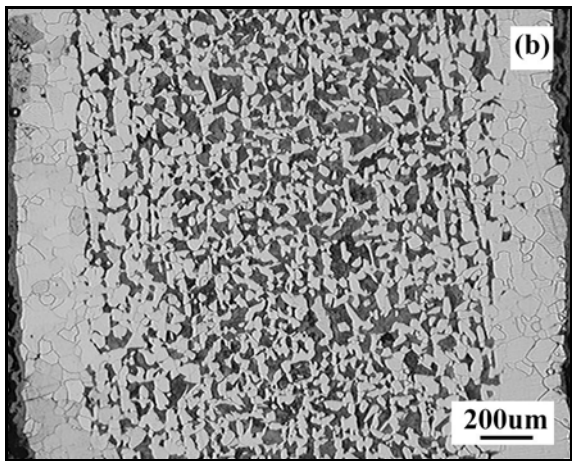

Fig. 6. Microstructure of 0.9%C-Fe steel at both sides of the specimen after 6 h at 930 °C: (a) $E = 4\,\mathrm{kV\,cm^{-1}}$ and (b) $E = 0\,\mathrm{kV\,cm^{-1}}$.

with 10 thickness measurements taken and averaged). The interface between fully and partially decarburized layers exhibits an arc-shaped boundary. Conversely, the interface between the non-electric field-induced fully decarburized layer and the partially decarburized layer appears irregular. The average thickness of the fully decarburized layer in the absence of an electric field measures 216 μm (based on a single field of view, with 10 thickness measurements taken and averaged).

Figure 6 illustrates the metallographic structure adjacent to the side surface of 0.9%C-Fe steel (indicated by the arrow in Fig. 3) after surface decarburization and oxidation at 930 °C for 6 h. In the image, the white regions depict ferrite, while the black areas represent lamellar pearlite (the core tissue of the sample was enlarged to 1000 times, as shown in Fig. 7). A comparative analysis of the metallographic structures following electric field and non-electric field heat treatments reveals a notable discrepancy in the thickness of the fully decarburized layer. As delineated in Table 2, the electrically field-heated sample exhibits a substan-

Table 2. Thickness of electric field and non-electric decarburization layer

Treatment mode	Observation position	Average thickness of full decarburization layer (μm)
Electric field (4 kV cm^{-1})	The sample end	553
	The sample edge	377
Non-electric field (0 kV cm^{-1})	The sample end	216
	The sample edge	207

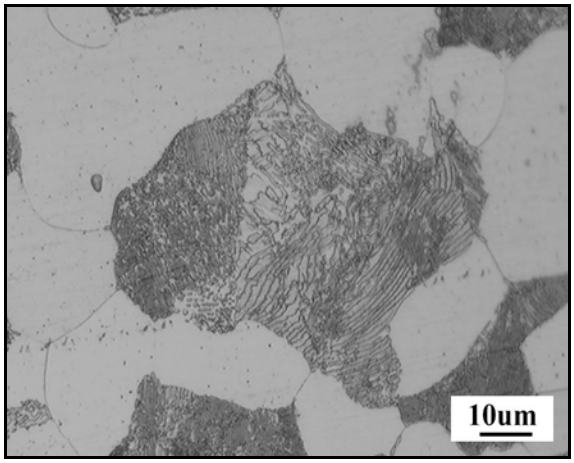

Fig. 7. Pearlite microstructures of 0.9%C-Fe steel heated at 930 °C for 6 h.

tially reduced thickness in the fully decarburized layer compared to its non-electrically field-heated counterpart. Specifically, the fully decarburized layer in the electrically field-heated sample measures 377 μm (averaged from 50 thickness values obtained across two selected fields of view), whereas the corresponding layer in the non-electrically field-heated sample is approximately 207 μm thick (average derived from 50 thickness values obtained across two selected fields of view).

Figure 8 depicts the microstructure at the core of the 0.9%C-Fe steel sample (as indicated by the arrow in Fig. 3) following a 6-hour exposure at 930 °C. Partial decarburization is observable in the core. Comparing the central regions of samples subjected to electric field-assisted heating and those without, a substantial increase in ferrite content is notable in the former. Furthermore, Figs. 5, 6, and 8 collectively reveal a consistent trend: distinctive differences in central morphology between samples treated with and without an electric field. Specifically, ferrite grain boundaries appear slightly rounded in the electrically heated samples, while those in the non-field-treated counterparts tend to exhibit angularity with a slight elongation.

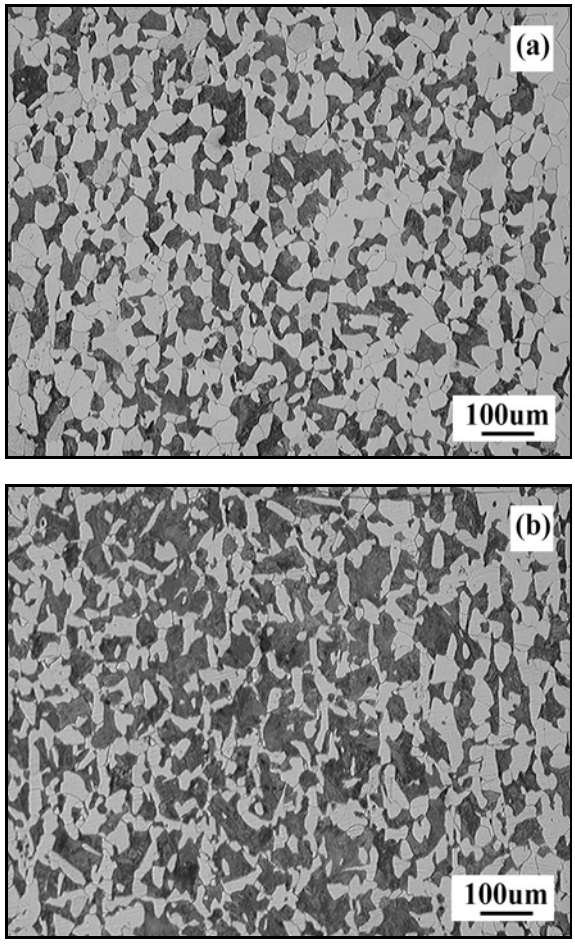

Fig. 8. Microstructures of the 0.9%C-Fe steel center heated at 930 °C for 6 h: (a) $E = 4\,\mathrm{kV\,cm^{-1}}$ and (b) $E = 0\,\mathrm{kV\,cm^{-1}}$.

4. Discussion

Decarburization of the steel surface encompasses two primary processes: carbon atom diffusion from the metal's interior to its surface and the oxidation reaction between the metal surface and oxygen in the furnace atmosphere. Upon reaching a specific temperature, the interaction between the steel surface and the furnace atmosphere or ambient air triggers a chemical reaction where carbon on the steel surface combines with oxygen, resulting in gas production. Consequently, a carbon concentration gradient forms between the interior and surface of the steel, intensifying the driving force for carbon diffusion. A comparative analysis of the decarburization layers of samples

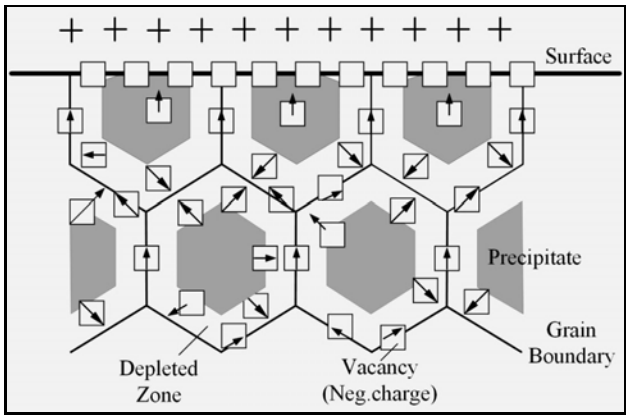

Fig. 9. Schematic illustration of the proposed model for the effect of an electric field on the quenching-aging of low-carbon steel [14].

heated with and without an electric field in this experiment reveals that the complete decarburization layer's thickness in samples subjected to electric field decarburization is greater than in those subjected to non-electric field decarburization. Moreover, a notable increase in ferrite percentage is observed in the sample's center (Figs. 5, 6, and 8). Consequently, it is evident that the total carbon content in samples heated with an electric field is lower than in those heated without it.

Fu [11] investigated the microstructure and diffusion behavior post-electric field heat treatment following friction welding of dissimilar metals. It was determined that applying an external electrostatic field can diminish the diffusion activation energy (Q) of iron elements at the friction welding interface during the friction welding process. During the heat treatment, Q fluctuates with variations in electric field intensity. Thus, it can be inferred that applying an electric field augments the diffusion coefficient of carbon atoms within the sample. According to the Arrhenius equation (Eq. (1)), assuming R and T remain constant, a decrease in diffusion activation energy Q increases the diffusion coefficient D. Therefore, the electric field's reduction of carbon atom diffusion activation energy accelerates the decarburization reaction rate:

$$D = D_0 \exp(-\frac{Q}{RT}), \tag{1}$$

where D is the diffusion coefficient, D_0 is the diffusion constant, Q is the diffusion activation energy, T is the absolute temperature, and R is the gas constant.

Many researchers [13, 14] posit that the electric field primarily influences the diffusion process through the vacancy mechanism. Conrad [14] employed Fig. 9 to vividly illustrate the migration pattern of atoms under an electric field. When a metal conductor is subjected to an external electric field, the free electrons within the conductor migrate in the direction of the electric field due to the influence of the electric field force, thus leading to a redistribution of charges within the conductor. Upon connecting the sample to the positive terminal of a power source, a significant accumulation of positive charge occurs on the sample's surface upon power application. During the vacancy migration process, the interaction between positive and negative charges diminishes the energy barrier for vacancy hopping. Conventionally, vacancies are perceived as negatively charged, facilitating the diffusion of vacancy complexes comprising carbon atoms + vacancies towards grain boundaries or surfaces, thereby expediting the diffusion of carbon atoms to the sample surface.

Additionally, Figs. 5, 6, and 8 exhibit a common observation: the morphology of proeutectoid ferrite differs between samples subjected to an electric field and those without. In electric field-treated samples, the proeutectoid ferrite grains at the center display slightly rounded edges with fewer corners, while in non-electric field-treated samples, the edges of proeutectoid ferrite grains within the magnetic core structure appear more elongated with additional edges. This discrepancy can be attributed to the decarburization process, where a portion of carbon diffuses into the atmosphere. Figures 5, 6, and 8 illustrate that after decarburization and slow cooling, the typical structure of hypereutectoid steel (secondary cementite) is absent, with a predominance of hypoeutectoid steel.

The 0.9%C-Fe steel sample's center post-decarburization transitions from hypereutectoid to hypoeutectoid steel. According to the iron-carbon phase diagram, hypoeutectoid steel first precipitates ferrite during cooling along the austenite grain boundary between the Ar3 and Ar1 lines. Decarburization intensifies upon applying an electric field, leading to lower carbon content and extended time for ferrite precipitation. Consequently, the volume content of preeutectoid ferrite increases, with grains growing along both austenite grain boundaries and within austenite grains. Thus, the morphology of proeutectoid ferrite becomes more rounded and indistinguishable from the original austenite grain outlines. Conversely, in non-electric field-treated samples with higher carbon content post-decarburization, proeutectoid ferrite precipitates primarily along austenite grain boundaries without sufficient time to infiltrate austenite grains, resulting in slightly elongated morphology with more pronounced edges and corners, distinctly visible along the austenite grain boundaries.

5. Conclusions

1. The electric field enhances the diffusion of carbon atoms to the surface of the sample, leading to an

average increase of 170 μm in the thickness of the fully decarburized layer. Thus, the electric field facilitates the decarburization process.

2. Following electric field annealing, the center of 0.9%C-Fe steel transforms into hypoeutectoid steel due to the ongoing diffusion of carbon towards the surface.

Acknowledgements

This work was supported by the National Natural Science Foundation of China (Grant Nos. 51771044, 51871042) and the Scientific and Technological Research Projects of Colleges and Universities in Hebei Province (Grant No. ZD2015213).

References

[1] Z. S. Zhou, M. Y. Dai, W. L. Wu, Z. Y. Shen, J. Hu, Effect of direct current field on salt bath nitriding kinetics for 35 steel, Transactions of Materials and Heat Treatment 36 (2015) 206–209. https://doi.org/10.13289/j.issn.1009-6264.2015.04.036

[2] R. Kapoor, S. Sunil, G. B. Reddy, S. Nagaraju, T. S. Kolge, S. K. Sarkar, Sarita, A. Biswas, A. Sharma, Electric current induced precipitation in maraging steel, Scripta Materialia 154 (2018) 16–19. https://doi.org/10.1016/j.scriptamat.2018.05.013

[3] Z. C. Wang, H. P. Yu, A. Liyanage, J. J. Qiu, D. Thushara, B. Bao, S. L. Zhao, Collective diffusion of charged nanoparticles in microchannel under electric field, Chemical Engineering Science 248 (2022) 117264. https://doi.org/10.1016/j.ces.2021.117264

[4] T. Chen, Y. Lei, Y. Li, D. B. Jia, T. P. Wen, G. Q. Liu, J. K. Yu, H. X. Li, Applied electric field on the reaction between submerged entry nozzle and alloy in the steel, Ceramics International 47 (2021) 22646–22653. https://doi.org/10.1016/j.ceramint.2021.04.278

[5] T. Ohnuma, Surface diffusion of Fe and Cu on Fe (001) under electric field using first-principles calculations, Microscopy and Microanalysis 25 (2019) 547–553. https://doi.org/10.1017/S1431927618015738

[6] X. Y. Zhang, L. Wang, Y. Wang, Y. Liu, X. D. Lv, Y. S. Chao, Effect of electrostatic-field treatment on the diffusion behaviors of Fe and Cr in GH4169 superalloy, Journal of Iron and Steel Research 23 (Supplement 2) (2011) 146–149. https://doi.org/10.13228/j.boyuan.issn1001-0963.2011.s2.039

[7] W. Liu, J. Z. Cui, The effect of homogenization treatment with an electric field on the microstructure and mechanical properties of 2091 Al-Li alloy, Acta Aeronautica et Astronautica Sinica 18 (1997) 324–329.

[8] W. Liu, K. M. Liang, Y. K. Zheng, J. Z. Cui, Study of the diffusion of Al-Li alloys subjected to an electric field, Journal of Materials Science 33 (1998) 1043–1047. https://doi.org/10.1023/A:1004380332280

[9] W. Liu, K. M. Liang, Y. K. Zheng, J. Z. Cui, Effect of an electric field during solution treatment of 2091 Al-Li alloy, Journal of Materials Science Letters 15 (1996) 1327–1329. https://doi.org/10.1007/BF00240796

[10] H. A. Lu, H. Conrad, Influence of an electric charge during quench aging of a low-carbon steel, Applied Physics Letters 59 (1991) 1847–1849. https://doi.org/10.1063/1.106191

[11] L. Fu, S. G. Du, Effect of external electric field on diffusion behavior of copper and stainless steel friction welded joint during post weld annealing treatment, Transactions of the China Welding Institution 25 (2004) 71–75.

[12] C. Lu, J. Yang, Y. Zhao, X. W. Lei, J. H. Huang, S. H. Chen, Z. Ye, Influence of applied electric field on atom diffusion behavior and mechanism for W/NiFe interface in diffusion bonding of Steel/NiFe interlayer/W by spark plasma sintering, Applied Surface Science 541 (2021) 148516. https://doi.org/10.1016/j.apsusc.2020.148516

[13] X. Y. Zhang, Effect of Electrostatic-field Treatment on the Diffusion and Segregation Behaviors of the Solute Atoms in GH4169 Superalloy, Master's thesis, Northeastern University, Shen Yang, China, July (2011).

[14] H. Conrad, Enhanced phenomena in metals with electric and magnetic fields: Electric field, Materials Transactions 46 (2005) 1083–1087. https://doi.org/10.2320/matertrans.46.1083